PCCP

Accepted Manuscript

ROYAL SOCIETY OF CHEMISTRY

www.rsc.org/pccp

ARTICLE TYPE www. rsc.org/xxxxxx | XXXXXXXX

Electronic structure at nanocontacts of surface passivated CdSe nanorods with gold clusters

Deepashri Saraf [a] **and Anjali Kshirsagar**[*a]

Received Xth XXXXXXXXXX 20XX, Accepted Xth XXXXXXXXX 20XX
First published on the web Xth XXXXXXXXXX 200X
DOI: 10.1039/b000000x

We report the electronic structure of free standing and gold attached passivated CdSe nanorods. The goal is to assess the changes at nanolevel after formation of contacts with gold clusters serving as electrodes and compare the results with experimental observations [Steiner *et al., Phys. Rev. Lett.*, 2005, **95**, 056805]. It is interesting to note that upon attaching gold clusters, the nanorods shorter than 27 Å develop metallicity by means of metal induced gap states (MIGS). Longer nanorods exhibit a nanoscale Schottky barrier emerging at the center. For these nanorods, interfacial region closest to the gold electrodes shows a finite density of states in the gap due to MIGS, which gradually decreases towards the center of the nanorod opening up a finite gap. Our theoretical results agree qualitatively with experimental results of Steiner *et al.* This study attempts to identify minimum length of a one-dimensional nanostructure to be used in an electronic device. An analysis of density of states and charge density brings out the role of hybridization of semiconductor states with metal states. Bader charge analysis indicates localized charge transfer from metal to semiconductor.

1 Introduction

Group II-VI semiconductors possess an ionic character which leads to larger band gaps and highly coordinated structures in bulk. This property differentiates them from other compound semiconductors in terms of size and structure dependent aspects at nanoscale. CdSe, being the most popular amongst them due to the reproducibility of its optical absorption and emission properties, has potential applications such as biosensors [1], displays [2] and quantum dot lasers [3]. Unique polar axis of hexagonal wurtzite geometry leads to one dimensional structures like nanorods which support a high density of excitons and offer the possibility of enhanced transport of dissociated charge carriers. Shape-controlled synthesis for CdSe nanorods has been reported in last decade [4–6]. Current synthesis techniques also allow for the diversity of geometric structures such as nanowires, nanobelts, nanotubes and nanorods.

Metal-semiconductor (M-S) interfaces and nanostructured systems are also gathering interest among the science community [7–11] due to their potential applications in developing electronic and optoelectronic devices. Recently, Bekenstein *et al.* have investigated and compared I-V characteristics of Cu_2S quantum dot core encapsulated by metallic Ru cage-like shell with individual components in a scanning tunneling spectroscopy study [12]. The geometry of multiply connected cage architecture has been shown to play a significant role in exhibiting single electron tunneling effects in empty cages [13] while a series of periodic negative differential conductance features are seen in the hybrid structures [12]. Trudeau *et al.* have studied charge transport in single CdTe nanocrystals in contact with Pd electrodes and have reported important implications of interface reactivity on electrical properties for integration of nanocrystals in conventional fabrication techniques [14].

The space-charge region in bulk M-S interfaces extends upto few nanometers. It is therefore fascinating to study nanostructures which physically are even less than few nanometers. The electronic properties of nanoscale counterpart of bulk M-S interfaces are yet to be understood completely. From the technological point of view, understanding the properties of such nanocontacts is a major step in the route towards the implementation of semiconductor nanocrystals (as well as molecules) in nanoelectronic device architectures. With the aim of finding answers to the specific issues pertaining to nanoelectronic device architectures, Landman *et al.* studied the M-S nanojunction problem theoretically [15]. They showed induction of subgap states near the Si-Al interface, decaying in Si nanowire and development of relatively large Schottky barriers in comparison to bulk. Demechenko and Wang calculated electronic structure of CdSe nanowires, in contact with metallic electrodes of experimentally relevant sizes, by incorporating the electrostatic image potential in atomistic single particle Schrödinger equation [16]. They demonstrated strong nanowire-size-dependence

[a]*Department of Physics and Center for Modeling and Simulation, University of Pune, Ganeshkhind, Pune 411007, India.* ***E-mail****: anjali@physics.unipune.ac.in*

of localized electron-hole states induced by the electrode.

In a scanning tunneling spectroscopy study of gold-tipped CdSe nanorods (nanodumbbell), Steiner *et al.* observed a gap similar to that in bare CdSe nanorods near the nanodumbbell center, while subgap structure is found near the M-S nanocontact[7]. They attributed this behaviour to the formation of subgap interface states that vanished rapidly towards the center of the rod, consistent with theoretical predictions given by Landman *et al.*[15]. The tunneling spectra can be correlated with the theoretical calculation of density of states (DOS). Theoretical predictions regarding range for decay of metal induced subgap states is about 1 nm according to Vostokov and Shashkin[17,18], while Landman *et al.* have shown in there calculations, that these states extend upto 0.5 nm[15] into the semiconductor. Experiments indicate that the subgap states exist even up to 5 nm from the interface[7]. The experimental estimates are dictated by spatial resolution and the fact that locality of tunneling spectra holds up to approximately the exciton-Bohr radius of material[7] ($\sim$ 5.6 nm for CdSe[19]). Present work is motivated by the experimental work of Steiner *et al.*

In present work, we study passivated CdSe nanorods of various lengths in order to see the effect of length variation on charge density profile of the rods. We also study their density of states profile upon formation of nanocontacts with gold clusters. We found that our results are qualitatively similar to those of Landman *et al.*[15] and Steiner *et al.*[7].

2 Computational details

Our calculations are based on density functional theory, implemented through Vienna Ab-initio Simulations Package[20] and are performed employing plane augmented wave[21] with exchange-correlation energy functional as given by Perdew, Burke and Ernzerhof[22]. The valence electronic configurations for Cd, Se and Au atoms are, $5s^2 4d^{10}$, $4s^2 4p^4$ and $6s^1 5d^{10}$ respectively. The cut-off energy used in plane wave expansion is 274.34 eV. The self-consistent convergence of energy is set to 10^{-5} eV. The calculations are performed only at a single *k*-point, namely the center of the Brillouin zone. Occupation numbers are treated according to the Fermi-Dirac scheme with a broadening of 0.001 eV. A sufficiently large unit cell is chosen for the free standing CdSe nanorods so that the minimum distance from the cluster boundary to unit cell boundary was 5 Å in each direction. This vacuum region is even larger (7 Å) for gold attached CdSe nanorods.

Surface atoms, due to lower co-ordination number, have incomplete bonding resulting in electronically active states, known as "dangling or unpassivated orbitals". These orbitals are localized and act as efficient traps for charge carriers. At nano-scale, materials become very sensitive to the surface properties due to high surface to volume ratio. Hence, surface passivation is essential for such semiconductor nanostructures. This removes the localized surface states from the band gap. It is experimentally evident that for the II-VI group heteropolar semiconductor nanostructures like CdSe; trioctylphosphine oxide (TOPO) or trioctylphosphine (TOP) are the right choice as passivating agents due to their optimal bonding to the nanostructure surface[23–25]. The complex and large atomic structures of these passivating agents are costly for computational calulations. Hence, one needs to explore simpler computational methods for surface passivation. There are various techniques developed for such calculations and each one has its own advantages and disadvantages[26–28]. For our calculations we use the technique developed by Huang *et al.*[29], where fictitious hydrogen atoms, H*, are chosen to complete the co-ordination of the surface atoms. The pseudopotentials for these pseudo-atoms with appropriate nuclear and valence charge, are generated using the Troullier-Martins prescription[30]. The authors suggest that CdSe dots with a wurtzite structure open a maximum band gap when H* atoms with valence electron charge Z = 1.5 are used to bond with Cd atoms (cations) and Z = 0.5 to bond with Se atoms (anions), thus maintaining the charge neutrality of the whole system.

To understand the structural stability, lattice-dynamical calculations (resulting in phonon DOS) are performed within the framework of self-consistent density functional perturbation theory. Force constant matrices thus obtained are used to generate vibrational frequencies of the system. In order to analyse the bonding between gold cluster and CdSe nanorods, Bader charge analysis method is used based on the algorithm developed by Henkelman *et al.*[31–33].

3 Results and Discussions

3.1 Cluster derived CdSe nanorods

CdSe nanorods are generated by relaxing a fragment (viz. Cd_3Se_3) of bulk wurtzite structure of CdSe crystal in $[\bar{1}\,0\,1\,0]$ direction, into its global minimum. This fragment has planar structure and can be considered as the basic building block of the longer nanorods (Cd_nSe_n). In this cluster, Cd atoms form an equilateral triangle of side 3.22 Å and Cd-Se bond length is 2.51 Å. Further, Cd_6Se_6 nanorod is constructed by stacking these six atom rings in chair conformation (See Figure 1-a(i)). This is the smallest nanorod under consideration. The atoms in this geometry relax in such a manner that intraplanar Cd-Se bond lengths are optimized to 2.60 Å, and Cd-Se interplanar

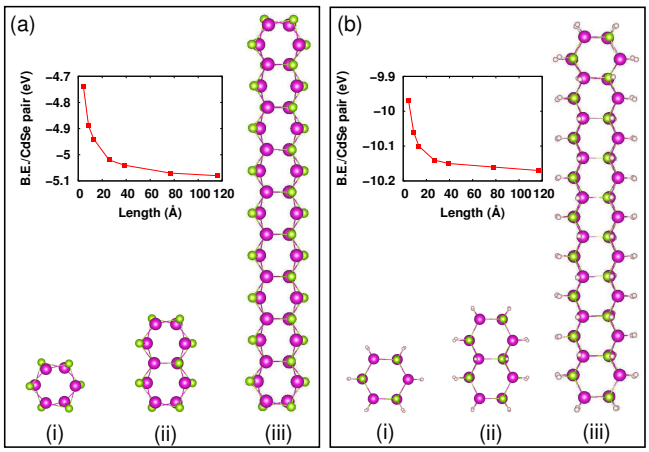

Fig. 1 (color online) Geometries of (a) bare and (b) passivated nanorods of various sizes (i) Cd_6Se_6 (4.34 Å, 4.64 Å), (ii) $Cd_{10}Se_{10}$ (8.65 Å, 9.04 Å) and (iii) $Cd_{38}Se_{38}$ (38.55 Å, 39.43 Å). Numbers in brackets indicate the lengths of the corresponding bare and passivated nanorods respectively. Cd, Se and H* atoms are indicated in magenta, green and pink respectively. The colour scheme is maintained throughout this article. Insets show the variation of BE per CdSe pair against lengths of the nanorods. Note the difference in the BE per CdSe pair scale on *y*-axis in (a) and (b).

bond lengths become 2.82 Å. The length of this nanorod is found to be 4.34 Å. The average width of the nanorod is 4.8 Å. The longer nanorods are then constructed by stacking Cd_6Se_6 units in a perpendicular direction through sharing of a Cd_2Se_2 unit (See Figure 1). This perpendicular stacking is found to be energetically more stable. Thus, we are dealing with the structures where all the atoms reside on the surface. Binding energy (BE) (defined as the difference between total energies of nanorods and the constituent atoms) indicate that structure is stable. As shown by the graph in the inset of Fig. 1(a), BE per CdSe pair reduces initially with the length of the nanorod and then saturates (See also Table 1). As the length increases the aspect ratio increases and BE per CdSe pair saturates.

For passivated CdSe nanorods, the wurtzite symmetry is maintained (See Figure 1(b)), but Cd-Se bond length is now elongated upto 2.71 Å and lengths increase slightly (maximum upto $\sim$ 0.9 Å) with respect to the unpassivated nanorods. Cd atoms bond with H* atoms with bond length 1.84 Å while Se-H* bond length is 1.60 Å. The structural stability of these nanorods is also confirmed using vibrational frequency analysis. Absence of imaginary frequencies establishes that the geometries of these nanorods are locally stable.

Table 1 gives the results of the calculations for passivated and unpassivated CdSe nanorods of different lengths. BE per CdSe pair for passivated structures indicates the same trend as that of unpassivated structures (See inset of Fig. 1(b)), but is lower for passivated structures with low aspect ratio. Thus, passivation takes care of the surface effects prevalent in structures of lower aspect ratios. Passivation moves the surface states present in the gap region either below the highest occupied molecular orbitals (HOMO) or above the lowest unoccupied molecular orbitals (LUMO) of the passivated structures retaining the intrinsic nature of corresponding states in unpassivated and passivated rods. This is evident from the local density of states (LDOS) of these structures. Hence, we could safely conclude that surface passivation is essential in case of such CdSe one dimensional structures. Inspection of band gap values of passivated nanorods shows a significant increase by upto 1.1 eV for the smallest length of nanorod. Thus, surface passivation removes the localized surface states from the gap region and these results contradict "self-healing" reported by Puzder *et al.*[34] in their study of CdSe clusters in the form of wurtzite cages of different diameters. In their work , Puzder *et al.* observe that the surface relaxation in CdSe nanostructures act in similar manner to that of passivated nanostructures of CdSe by opening the gap substantially.

Table 1 Comparison between the results for unpassivated (Bare) and passivated (+H*) nanorods.

Structures	Length (Å)		Band gap (eV)		BE per pair (eV)	
	Bare	+H*	Bare	+H*	Bare	+H*
Cd_6Se_6	4.34	4.64	2.02	3.17	-4.74	-9.97
$Cd_{10}Se_{10}$	8.65	9.04	1.98	2.99	-4.89	-10.06
$Cd_{14}Se_{14}$	12.91	13.50	2.03	2.94	-4.94	-10.10
$Cd_{26}Se_{26}$	25.76	26.60	1.99	2.71	-5.02	-10.14
$Cd_{38}Se_{38}$	38.55	39.43	1.95	2.52	-5.04	-10.15
$Cd_{74}Se_{74}$	76.96	77.78	1.88	2.42	-5.07	-10.16
$Cd_{110}Se_{110}$	115.85	116.66	1.87	2.35	-5.08	-10.17

Figures 2(a) and (b) show the partial charge density plots for HOMO and LUMO of passivated CdSe nanorods respectively. The partial charge density distribution of HOMO is predominantly localized on Se atoms which comes from the p_y orbitals (which lie along the length of the rod) of the atoms while that of LUMO is on both Cd and Se atoms arising from *s* orbitals of both Cd and Se throughout the nanorod. This is also reflected in the site projected DOS (See Figure 3). For short nanorods, (<15 Å), p_z orbitals of Se atoms at the edges also contribute to HOMO. The range of partial charge density arising from HOMO saturates at 39 Å for longer rods.

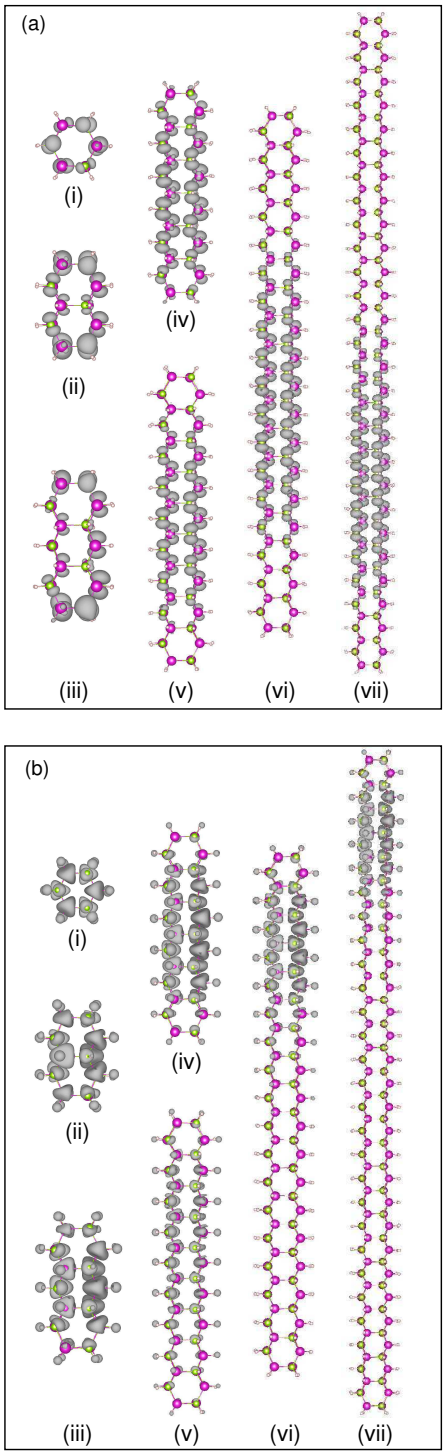

Fig. 2 Partial charge densities of the nanorods showing states HOMO in (a) and LUMO in (b). Note the presence of *p*-states in HOMO on Se atoms while *s* as well as *p*-states in LUMO on Cd and Se atoms.

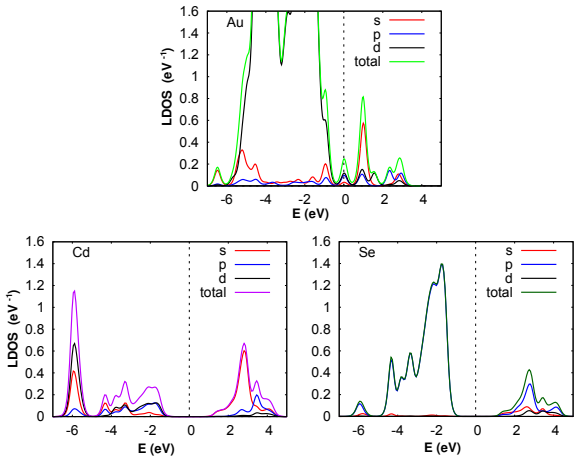

Fig. 3 Site projected DOS of Au atom in gold cluster (Au_{13}) and Cd and Se atoms in free standing passivated nanorods (Cd_nSe_n). Note the dominant presence of *p* states of Se in HOMO and *s* and *p* states of Cd as well as Se in LUMO.

In case of LUMO, as the length of the nanorods increases, the contribution to the partial charge density from Cd atoms, goes on decreasing. The span of LUMO saturates over the length of 30 Å. The passivating agents show the contribution from *s* orbitals in the LUMO of the nanorods. Bader charge analysis shows that the bonding between Cd and Se atoms in the nanorods has a partial ionic character with Cd transferring an average charge of 0.55*e* on Se.

3.2 Gold tipped CdSe nanorods

Global minimum geometry of Au_{13} cluster is found to be suitable to attach at the ends of the nanorods. In this cluster, gold atoms are arranged in three distinct planes. The bare clusters are attached to relaxed nanorods. These compound structures are then optimized fully forming a dumbbell-like structure (nanodumbbell). We observe that the nanorods are unaffected due to the end passivation by gold electrodes, except at the M-S nanojunctions, where CdSe bond length elongates to increase the area of the quadrilateral formed by two CdSe pairs. Geometry of gold cluster however changes significantly (See Figures 4(ii) and (iii)). We can observe a slight buckling in three planes of the cluster towards M-S interface. Both Cd and Se atoms at the ends of the nanorods are doubly bonded to the Au atoms at the junctions, where Au-Cd and Au-Se average bond lengths are 2.74 Å and 2.85 Å respectively.

LDOS calculated for every plane of the gold tipped

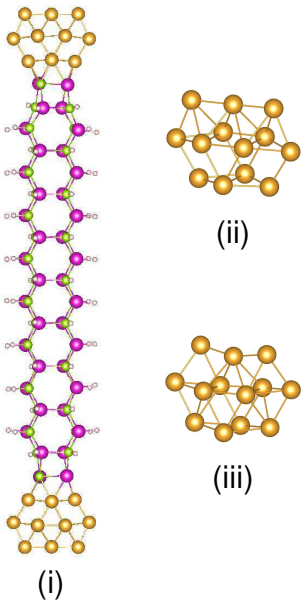

Fig. 4 (i) Gold (Au_{13}) tipped passivated $Cd_{38}Se_{38}$ nanorod. Au atoms are indicated in yellow. Au_{13} clusters : (ii) bare and (iii) upon attaching at the tips of CdSe nanorods. Notice the buckling in the geometry upon attaching at the tips of the rods. Gold atoms at the interface are bonded to Cd as well Se atoms at the tips of the rods.

nanorods (See Figure 5), shows a gap near nanodumbbell center and metal induced gap states (MIGS) emerge near M-S nanocontact. These MIGS vanish rapidly towards the center of the nanorod[7,15]. For short nanorods (upto $\sim$ 27 Å) bridging gold electrodes, we find full metallization by these MIGS (Fig. 5(a), (b), (c) and (d)), while for longer nanorods, we find a gap-structure emerging away from M-S junction. For longer nanorods, in interfacial regions closest to the metal electrodes, a finite LDOS is observed in the gap indicating a metallic nature which gradually decays away from the electrode. A comparison of site projected DOS of gold attached nanorods and their separated components (See Figure 3), shows the hybridization of metal states with semiconductor states. There is maximum opening of the gap at the central plane of nanodumbbell and the gap size decreases with increasing length of the nanorod, eventually saturating to a value 2.05 eV. Figure 6 shows plane-wise site projected LDOS for $Au_{13}Cd_{38}Se_{38}Au_{13}$ nanodumbbell where MIGS start vanishing rapidly across the planes and central plane of the rod shows the presence of only semiconductor states. MIGS are present only upto a distance of $\sim$ 15.5 Å from the interface, thus making it clear why the nanorods shorter than 27 Å show full metallization. In case of Si-Al nanocontacts, Landman *et al.* have shown that these MIGS extend upto 5 Å from the interface in the Si region for Si

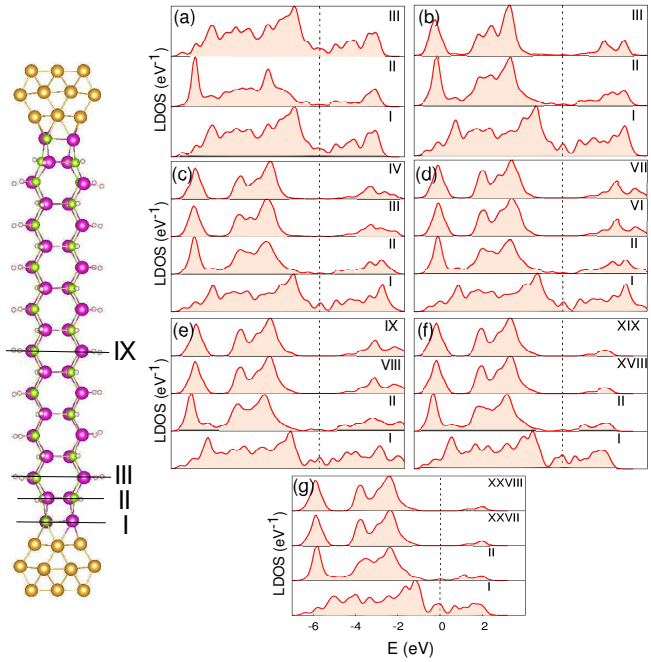

Fig. 5 (color online) LDOS corresponding to various planes, as depicted on the left for gold (Au_{13}) tipped passivated $Cd_{38}Se_{38}$ nanorod, are shown for following nanorods : (a) Cd_6Se_6, (b) $Cd_{10}Se_{10}$, (c) $Cd_{14}Se_{14}$, (d) $Cd_{26}Se_{26}$, (e) $Cd_{38}Se_{38}$, (f) $Cd_{74}Se_{74}$ and (g) $Cd_{110}Se_{110}$. The Fermi level (shifted to zero of energy) is marked by the vertical dotted line. Each plane in the nanorod contains two CdSe pairs along with their passivating H* atoms. Numbering is done only up to the central plane owing to the symmetry of the geometry as well as the electronic structure of nanorods (as is evident in (a) for planes I and III). LDOS shows MIGS present at the central plane in structures (a), (b), (c) and (d). These states are absent around the central planes of (e), (f) and (g). The HOMO-LUMO gap at the central plane for these nanorods increases and saturates for longer rods.

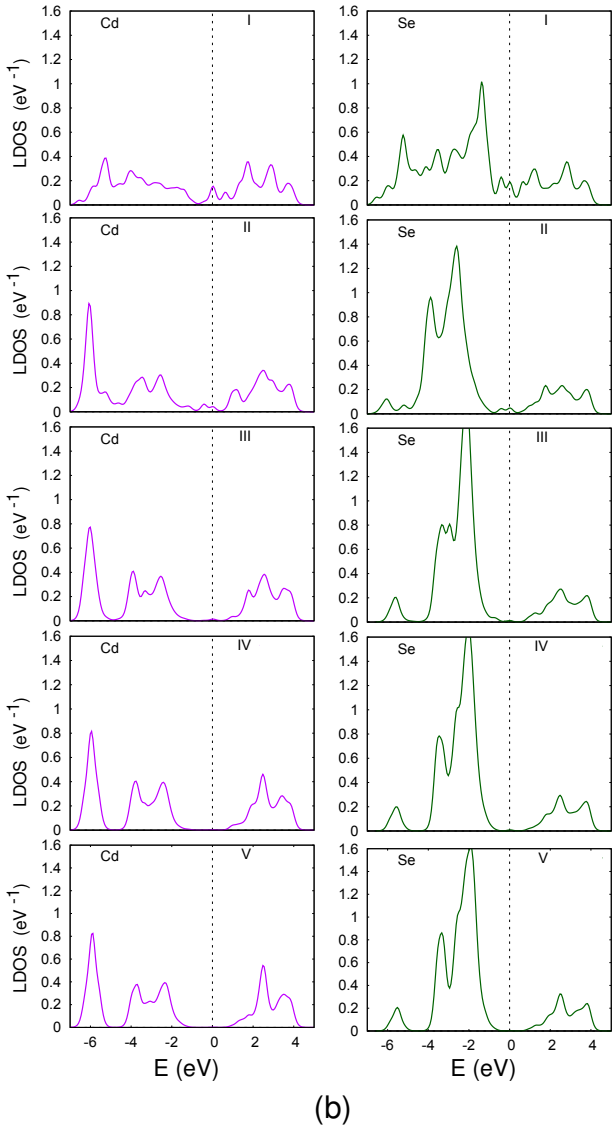

Fig. 6 Plane-wise site projected DOS of Cd atoms in left column and Se atoms in right column, in gold tipped $Cd_{38}Se_{38}$ rod. In the plane near the junction, one can see the presence of hybridized gold states in the gap. These states are also present over a wide energy scale below HOMO, indicating hybridization. Gold states are drastically reduced in the very next plane. As we go towards the center of the rod, the DOS does not show the presence of gold states and the DOS profile of Cd and Se looks the same as that of free standing passivated CdSe nanorod (As shown in Fig. 3).

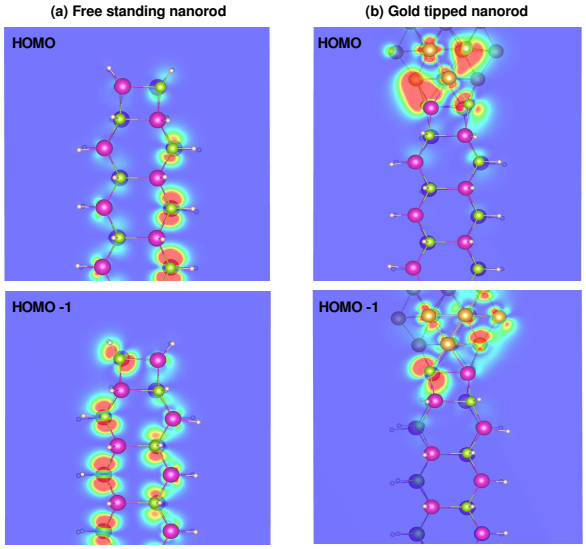

Fig. 7 Partial charge density contour plots for HOMO and HOMO-1 states of (a) free standing and (b) gold tipped passivated $Cd_{38}Se_{38}$ nanorod.

rods of lengths 25Å and diameter 2.5 Å[15]. Landman *et al.* find shorter rods of length 6Å and diameter 2.5Å to be fully metallized when ends are capped with Al clusters[15].

Figure 7 depicts the partial charge density plots for HOMO and HOMO-1 states for free standing and gold attached passivated $Cd_{38}Se_{38}$ nanorod. For the nanodumbbells, the HOMO and HOMO-1 states are comprised of gold *d* and *s* states hybridized with p_z states of Se and *s* states of Cd as shown in Fig. 7(b). This behaviour is also evident from the LDOS plots in Fig. 6. Hybridization of gold states with Cd states is not evident in the partial charge density plots. However, gold induced states appear around Cd atoms in the contact plane (See Fig. 6 - Plane I and II). The p_y states of Se atoms comprising the HOMO and nearby levels in free standing passivated $Cd_{38}Se_{38}$ nanorod have shifted below Fermi level (E_F) by $\sim$2 eV, while states near HOMO in gold tipped nanorod mainly arise from gold and are spatially localized near the contact plane. Bader charge analysis for the nanodumbbells shows that changes in the charge transfer in comparison to free standing rods are localized near the interface. Bonding remains same away from the interface. At the interface, Cd atoms transfer an average charge of 0.68*e* while Se atoms acquire an average charge of 0.53*e*. The remaining charge gets distributed on the gold cluster. There is marginal difference in the charge transfer to Se atoms in free standing and gold attached nanorods, however, charge transfer from Cd atoms has considerably increased in gold

Table 2 Schottky barrier height (SBH) and HOMO-LUMO gap at the central plane as a function of the length of CdSe nanorods. SBH for bulk gold-CdSe contacts is 0.7 eV at 300 K[35].

Structures	Length (Å)	Schottky barrier height (eV)	Gap at central plane (eV)
$Cd_{38}Se_{38}$	39.43	1.00	2.12
$Cd_{74}Se_{74}$	77.78	0.92	2.06
$Cd_{110}Se_{110}$	116.66	0.93	2.05

attched nanorods.

Difference in work function of metal (Au) and electron affinity of semiconductor (CdSe) yields a Schottky barrier when the two are brought in contact. A decrease in the number of available states in confined structures causes an increase in the energy barrier that carriers have to surmount in order to cross the interface. Quantum confinement of carriers is known to increase the minimum energy that a carrier has to have (relative to HOMO for electrons and LUMO for holes) to propagate.

For an n-type semiconductor like CdSe, the Schottky barrier height (SBH) is given by the difference between the metal work function and the electron affinity of the semiconductor. This is calculated from the position of E_F in the nanodumbbell and the position of LUMO in the middle section of the CdSe nanorod following Landman *et al.*[15]. The values for SBH are listed in Table 2. We find SBH to be 30 to 43 % higher than the bulk value as opposed to 40 to 90 % for Si-Al interface as reported by Landman *et al.*[15]. It may be noted the authors have carried out the calulations only for two sizes of Si nanorods and the diameter of their nanorods is 2.5 Å. Smaller SBH values are preferred when metal contacts are to be used as electrodes in device fabrication while larger SBH values are required if the M-S hybrid is to be used as a Schottky diode.

Group II-VI semiconductors have a higher component of ionic bonding and hence these materials do not create large number of surface states. Their barrier heights therefore depend upon the work function of the metal. Here, the SBH for longer nanorods, which do not show metallization, saturate for the nanorods having lengths longer than ∼78 Å.

4 Conclusions

In summary, we report that passivation of CdSe nanorods opens up the band gap considerably and we do not observe any "self-healing" as reported by Puzder *et al.*[34] for 3-dimensionally (3D) confined structures. For free standing nanorods contribution to HOMO comes mainly from *p* orbitals of Se similar to bulk and 3D confined structures. However contribution to LUMO comes from *s* orbitals of Cd and Se while for bulk and 3D confined structures LUMO mainly consists of Cd *s* states. For longer nanorods the spatial extent of partial charge densities saturates. HOMO is confined over a region of 39 Å, while LUMO is confined over 30 Å. Gold attached nanorods are fully metalized for shorter lengths ($<$ 27 Å), while they develop a Schottky barrier, larger than the bulk value (0.7 eV at 300 K[35]), for longer nanorods, where a semiconducting band gap starts to show up at a distance of 15.5 Å from the nanojunction. A comparison of gold attached nanorods and their separated components show charge transfer which is highly localized at contact region. For the nanorods studied in this work (width 4.8 Å), we identify the minimum length of the nanorod to be ∼30 Å to be useful in an electronic device by retaining its semiconducting nature.

5 Acknowledgements

All the figures of the structures are generated using VESTA[36]. We thank Department of Science & Technology, Government of India for financial support (Grant code : DST/INT/SWISS/P-36/2012 and SR/NM/NS-15/2011(G)) and C-DAC, Pune for use of their computing facilities.

References

1 W. C. Chan and S. Nie, *Science*, 1998, **281**, 2096.
2 V. L. Colvin, M. C. Schlamp and A. P. Alivisatos, *Nature*, 1994, **370**, 354.
3 V. I. Klimov, *Science*, 2000, **290**, 314.
4 J. Hu, L. Li, W. Yang, L. Manna, L. Ang and A. P. Alivisatos, *Science*, 2001, **292**, 2060.
5 X. Peng, *Adv. Mater.*, 2003, **15**, 459.
6 A. S. Barnard, X. Huifang, L. Xiaochun, N. Pradhan and X. Peng, *Nanotechnology*, 2006, **17**, 5707.
7 D. Steiner, T. Mokari, U. Banin and O. Millo, *Phys. Rev. Lett.*, 2005, **95**, 056805.
8 R. de Paiva and R. D. Felice, *Am. Chem. Soc. NANO*, 2008, **2**, 2225.
9 T. Mokari, C. G. Sztrum, A. Salant, E. Rabani and U. Banin, *Nature Materials*, 2005, **4**, 855.

10 A. Salant, E. Amitay-Sadovsky and U. Banin, *J. Am. Chem. Soc.*, 2006, **128**, 10006–10007.
11 R. Costi, A. E. Saunders, E. Elmalem, A. Salant and U. Banin, *Nano Letters*, 2008, **8**, 637.
12 Y. Bekenstein, K. Vinokurov, U. Banin and O. Millo, *Nanotechnology*, 2012, **23**, 505710.
13 Y. Bekenstein, K. Vinokurov, T. J. Levy, E. Rabani, U. Banin and O. Millo, *Phys. Rev. B*, 2012, **86**, 085431.
14 P.-E. Trudeau, M. Sheldon, V. Altoe and A. P. Alivisatos, *Nanoletters*, 2008, **8**, 1936.
15 U. Landman, R. N. Barnett, A. G. Scherbakov and P. Avouris, *Phys. Rev. Lett.*, 2000, **85**, 1958.
16 D. O. Demechenko and L. W. Wang, *Nano Lett.*, 2007, **7**, 3219.
17 N. V. Vostokov and V. I. Shashkin, *J. Exp. Theor. Phys.*, 2003, **99**, 211.
18 N. V. Vostokov and V. I. Shashkin, *Semiconductors*, 2004, **38**, 1047.
19 R. W. Meulenberg, J. R. I. Lee, A. Wolcott, J. Z. Zhang, L. J. Terminello and T. Buuren, *ACS Nano*, 2009, **3**, 325.
20 G. Kresse and J. Furthmuller, *Phys. Rev. B*, 1996, **54**, 11169.
21 P. E. Blochl, *Phys. Rev. B*, 1994, **50**, 17953.
22 J. P. Perdew, K. Burke and M. Ernzerhof, *Phys. Rev. Lett.*, 1996, **77**, 3865.
23 A. P. Alivisatos, *Science*, 1996, **271**, 933.
24 J. M. Heath, *Acc. Chem. Res.*, 1999, **32**, 38.
25 P. Yang, S. Tretiak, A. E. Masunov and S. Ivanov, *J. Chem. Phys.*, 2008, **129**, 074709.
26 L. W. Wang and A. Zunger, *Phys. Rev. B*, 1996, **53**, 9579.
27 K. Shiraishi, *J. Phys. Soc. Jpn.*, 1990, **59**, 3455.
28 J. W. Wang and J. Li, *Phys. Rev. B*, 2004, **69**, 153302.
29 X. Huang, E. Lindgren and J. R. Chelikowsky, *Phys. Rev. B*, 2005, **71**, 165328.
30 N. Troullier and J. L. Martins, *Phys. Rev. B*, 1991, **43**, 1993.
31 W. Tang, E. Sanville and G. Henkelman, *J. Phys.: Condens. Matter*, 2009, **21**, 084204.
32 E. Sanville, S. D. Kenny, R. Smith and G. Henkelman, *J. Comp. Chem.*, 2007, **28**, 899.
33 G. Henkelman, A. Arnaldsson and H. Jonsson, *Comput. Mater. Sci.*, 2006, **36**, 254.
34 A. Puzder, A. J. Williamson, F. Gygi and G. Galli, *Phys. Rev. Lett.*, 2004, **92**, 217401.
35 S. M. Sze and K. K. Ng, *Physics of Semiconductor Devices*, John Wiley and Sons, Inc., New Jersey, 2007.
36 K. Momma and F. Izumi, *J. Appl. Crystallogr.*, 2008, **41**, 653.